Supporting Information

Shi et al. 10.1073/pnas.1012596108

Results.

DhaK–DhaL Binding Interface. Upon complex formation, the buried surface for DhaK is 1,223 Å^2 or 8.6% of the total solvent-accessible surface (14,150 Å^2) of the DhaK subunit. The buried surface for DhaL due to complex formation is 1,346 Å^2, accounting for 14.9% of the total solvent-accessible surface of DhaL (9,010 Å^2).

The hydroxyl group of Tyr181^L forms a water-mediated H bond with the backbone carbonyl oxygen of Asn105^K, whereas the Tyr181^L aromatic ring stacks against the side chains of Tyr106^K and Arg148^K that are otherwise buried in the uncomplexed DhaK structure. The residues preceding Tyr181^L also form favorable interactions with the relocated loop $\beta6^K/\alpha4^K$ (Fig. 1*C*). For example, the side chain of Arg175^L packs against the aromatic ring of Tyr143^K and the hydroxyl group of Ser180^L forms an H bond with the amide group of Ala145^K. On the C-terminal side of Tyr181^L, in addition to hydrogen bonding to the carbonyl group of Gly222^K, Arg185^L is neutralized by Glu212^K through a salt bridge. Except for the loop $\alpha7^L/\alpha8^L$, other regions of DhaL also contribute H bonds to stabilize the complex (Fig. 1*C*). The carboxylate of Asp37^L is within H-bonding distance of the hydroxyl group of Thr79^K. The amide and carbonyl groups of Gly78^L, which are situated in the loop $\alpha3^L/\alpha4^L$ and are in close vicinity of the ADP β-phosphate, make hydrogen bonds to the main chain carbonyl of Ser80^K and the side chain of Asn112^K, respectively. The guanidinium group of Arg120^L, located at the end of $\alpha5^L$, is anchored by the hydroxyl of Thr115^K.

Comparison of the *E. coli* DhaK–DhaL Complex, the *C. freundii* Dha Kinase and the *L. lactis* DhaL-DhaM Complex. The overall structure of both DhaK and DhaL subunits in the *E. coli* complex are similar to the corresponding domains of the *C. freundii* Dha kinase (1). However, the binding interface between these two subunits/domains is quite different in the two kinases (Fig. S1*A*). The assembly in *C. freundii* is likely driven by the hydrophobic nature of the interface and further strengthened by the long linker between the two domains. This differs from the dominant polar nature of the corresponding contact areas in the DhaK–DhaL complex in *E. coli* (Fig. 1*C*). In contrast to the rigidity shown by the loop $\alpha7^L/\alpha8^L$ capping the ADP binding site in both free and complexed *E. coli* DhaL subunits, the corresponding region in the nucleotide-binding domain of *C. freundii* Dha kinase is disordered even in the presence of bound AMP-PNP. This is consistent with the different roles of the nucleotide in these two systems (2): ADP in the PTS-dependent kinase functions as a coenzyme and remains permanently bound, whereas ATP is a substrate and needs to be recruited in each catalytic cycle in the *C. freundii* kinase. Recently, the crystal structure of the DhaL-DhaM complex from *L. lactis* has been reported (3). The DhaM protein has the EDD fold (4), which is also the core structure of DhaK. As expected, the DhaL subunit in this complex shares high similarity with that in the *E. coli* DhaK–DhaL complex with an rmsd of 1.1 Å for the aligned 179 Cα atoms (Fig. S1*B*). Unlike the DhaK subunit in our DhaK–DhaL complex, the DhaM subunit from *L. lactis* does not undergo significant conformational adjustments upon complex formation. Based on similarities between DhaM and DhaK, such as the positions of several conserved polar residues, a model for the *L. lactis* DhaK–DhaL complex has been proposed (3). In this model, salt-bridge interactions were predicted to play important roles in DhaK–DhaL complex formation. These salt-bridge interactions, involving a few specific residues, however, are not present in our DhaK–DhaL complex structure even though most of these charged residues are conserved, including Arg120^L and Lys122^L as well as Glu114^K and Glu118^K. In both free and DhaL-bound *E. coli* DhaK, the carboxylate group of Glu114^K is fixed by the salt-bridge provided by Arg253^K, whereas that of Glu118^K is anchored by Trp262^K, the latter of which is part of the well-conserved Trp zipper in the β-hairpin capping the edge of the N-terminal β-sheet of DhaK (Fig. S8). This structural arrangement prevents the involvement of Glu114^K and Glu118^K in interacting with DhaL. It is also very likely that *L. lactis* DhaK/L complex formation will be accompanied by similar conformational changes for *L. lactis* DhaK as seen in *E. coli* DhaK.

Materials and Methods.

Protein Cloning, Mutagenesis, Expression, and Purification. The *dhaK* (gi: 87081857), *dhaL* (gi: 1787449) and *pstH* (phosphocarrier protein HPr gi: 1788755) genes from *Escherichia coli* K12 were cloned into a modified pET15b vector (Novagen) that resulted in an N-terminal His$_8$-tag fusion protein with a tobacco etch virus (TEV) protease site used to remove the tag. The *dhaM* (gi: 87081856) and *ptsI* (phosphotransferase system Enzyme I gi: 1788756) genes from *E. coli* K12 were cloned into a modified pGEX-4T1 vector (Pharmacia) to create an N-terminal GST-fusion protein followed by a TEV protease site. Site-directed mutagenesis was carried out using the QuikChange mutation kit (Stratagene) according to the manufacturer's protocol and were confirmed by DNA sequencing. Transformed *E. coli* BL21 (DE3) cells were grown at 37 °C in Luria-Bertani (LB) broth with 100 μg/mL ampicillin and induced with 0.5 mM isopropyl β-D- thiogalactopyranoside at 22 °C for 16–20 hours.

For DhaK constructs, cells were resuspended in buffer A (50 mM Tris pH 8 and 300 mM NaCl) with 10 mM imidazole and 1 mM DTT and lysed by sonication. Cleared lysates were applied to nickel-nitrilotriacetic acid (Ni-NTA) resin and washed with buffer A containing 20 mM imidazole and 1 mM DTT. Proteins were eluted with 200 mM imidazole and 1 mM DTT in buffer A. DhaL constructs were purified in a similar manner, except that 1 mM magnesium acetate and 1–100 μM ADP (2) or AMP-PNP (Sigma) were added to all buffers. DhaK constructs were dialyzed against buffer B (50 mM Tris pH 8, 150 mM NaCl and 1 mM DTT) and the His$_8$-tags were cleaved by TEV protease. The resulting protein was applied to Ni-NTA resin to remove His-tagged TEV protease and any uncleaved protein.

To verify that the kinase mutants (H56A^K, H56N^K, D109A^K, D109N^K, H218K^K, R178E^L) retained their ability to form the DhaL–DhaK complex, samples were analyzed by gel filtration (Superdex 200) in low salt buffer (20 mM Tris pH 8, 10 mM NaCl, 1 mM DTT) with 1 mM magnesium acetate and 1 μM ADP. Prior to gel filtration, samples containing one wild-type subunit and one mutant subunit (1 : 1 molar ratio) were dialyzed against the low salt buffer containing 1 mM magnesium acetate and 10 μM ADP. Complex formation was observed as an increase in mass resulting from a slight shift in elution volume (14.05–14.54 mL) when compared to the elution profile of DhaK alone (14.86 mL). Peak fractions were also analyzed by SDS/PAGE to confirm the presence or absence of both subunits.

For purification of Enzyme I and DhaM, cells were resuspended in buffer C (1× PBS with 300 mM NaCl and 1 mM DTT) and lysed by sonication. Cleared lysates were applied to Glutathione-sepharose resin and washed with buffer C. The proteins were eluted by TEV cleavage where the column was washed with buffer A followed by an overnight incubation in buffer B

containing TEV (100 μg/mL). TEV was removed by passing the sample through Ni-NTA resin.

HPr was found to be insoluble and therefore purified from inclusion bodies. Cell pellets were resuspended in buffer A and washed with 1% Triton X-100 based on the General Protocol by Burgess (5). Inclusion bodies were resuspended in 8 M urea (rocked 3 hours at room temperature) and applied to Ni-NTA. The resin was washed with 8 M urea followed by washing with buffer A. Soluble HPr was eluted with 200 mM imidazole in buffer A.

For crystallization the His_8-tag was cleaved from DhaL in a manner similar to DhaK except that 1 mM magnesium acetate and 1 μM of AMP-PNP were added to buffer B. DhaK and DhaL were mixed in a 1 : 1 molar ratio and dialyzed into buffer containing 50 mM Tris pH 8, 10 mM NaCl, 1 mM DTT, 1 mM magnesium acetate and 1 μM AMP-PNP. Protein samples were further purified on a Superdex 200 column equilibrated in the same buffer. Fractions containing the DhaK–DhaL complex were concentrated to 10 mg/mL by ultrafiltration and 0.2 mM PMSF was added. No density corresponding to AMP-PNP was observed in the complex.

NMR-based Phosphotransferase Assays. ^{1}H NMR was used to directly detect formation of Dha-P, alleviating the necessity of using a coupled assay with glycerol-3-phosphate dehydrogenase. Reaction conditions were very similar to those for the spectrophotometric assay, including enzyme concentrations, buffers and temperature except that 3 mM PEP and 1.6 or 16 mM Dha was used as substrate. NMR spectra were acquired at 600 MHz using an AVANCE III spectrophotometer (Bruker) equipped with a cryoprobe. Chemical shifts for Dha and PEP were established using pure compounds. Representative spectra are shown in Fig. S6.

Molecular Dynamics Simulations. The DhaK–DhaL–(ATP), DhaK–DhaL–(*syn*-ADP), and DhaK-–DhaL–(*anti*-ADP) complexes were sampled by 5-ns MD simulations using the AMBER10 suite of programs (6) together with the AMBER ff03 force field for proteins and a modified force field for ATP and ADP (7). Starting from the crystal structure of the DhaK–DhaL–(ADP) complex, the γ-phosphate group was attached to ADP in the crystal structure to form the ATP substrate using the Leap program in AMBER10 utilizing the ATP library file of Meagher et al. (7). The *syn*-ADP starting structure was adapted from the ADP-bound DhaL crystal structure (2BTD) (8) and superposed onto the crystal structure of the DhaK–DhaL–(ADP) complex (PDB ID code 3PNL). RESP (Restrained ElectroStatic Potential) partial charges for Dha covalently bound to $His218^K$ were calculated. Each complex was solvated in a rectangular parallelepiped TIP3P water box (9) and the electro-neutrality of the system achieved by the addition of Na^+ counter ions. For the ATP-bound complex, the nucleophilic hydroxyl Oγ atom of Dha was subjected to two harmonic distance restraints of 30 kcal mol^{-1} Å^{-2}, one with respect to the reactive γ-phosphate P atom of ATP within the 3.4–3.9 Å range and the other one to the OD2 atom of $Asp109^K$ of DhaK within the 2.7–3.2 Å range. For the ADP-bound complex, only the second restraint was used. The two Mg^{2+} ions in the crystal structure were subjected to harmonic distance restraints with respect to their coordinating atoms from $Asp30^L$, $Asp35^L$, $Asp37^L$, $Phe78^K$ and the α- and β-phosphate groups of ATP or ADP. For each complex, we performed a 5 ns NPT production run with snapshots collected every 1 ps, using a 2 fs time-step. The final ATP or ADP-bound complex structure was obtained by coordinate averaging over the last 2 ns of the MD trajectory, followed by 1,000 steps of energy minimization without any restraints.

1. Siebold C, Arnold I, Garcia-Alles LF, Baumann U, Erni B (2003) Crystal structure of the *Citrobacter freundii* dihydroxyacetone kinase reveals an eight-stranded alpha-helical barrel ATP-binding domain. *J Biol Chem* 278: 48236–48244.
2. Bachler C, Flukiger-Bruhwiler K, Schneider P, Bahler P, Erni B (2005) From ATP as substrate to ADP as coenzyme: Functional evolution of the nucleotide-binding subunit of dihydroxyacetone kinases. *J Biol Chem* 280:18321–18325.
3. Zurbriggen A, et al. (2008) X-ray structures of the three *Lactococcus lactis* dihydroxyacetone kinase subunits and of a transient intersubunit complex. *J Biol Chem* 283: 35789–35796.
4. Kinch LN, Cheek S, Grishin NV (2005) EDD, a novel phosphotransferase domain common to mannose transporter EIIA, dihydroxyacetone kinase, and DegV. *Protein Sci* 14: 360–367
5. Burgess, RR (2009) Refolding solubilized inclusion body proteins. *Method Enzymol* 463: 259–282.
6. Case DA, et al. (2005) The Amber biomolecular simulation programs. *J Comput Chem* 26:1668–1688.
7. Meagher KL, Redman LT, Carlson HA (2003) Development of polyphosphate parameters for use with the AMBER force field. *J Comput Chem* 24:1016–1025.
8. Oberholzer AE, Schneider P, Baumann U, Erni B (2006) Crystal structure of the nucleotide-binding subunit DhaL of the *Escherichia coli* dihydroxyacetone kinase. *J Mol Biol* 359:539–545.
9. Jorgensen WL, Chandrasekhar, J Madura JD, Impey, RW, Klein ML (1983) Comparison of simple potential functions for simulating liquid water. *J Chem Phys* 79:926–935.
10. Siebold C, Garcia-Alles LF, Erni B, Baumann U (2003) A mechanism of covalent substrate binding in the x-ray structure of subunit K of the *Escherichia coli* dihydroxyacetone kinase. *Proc Natl Acad Sci USA* 100: 8188–8192.

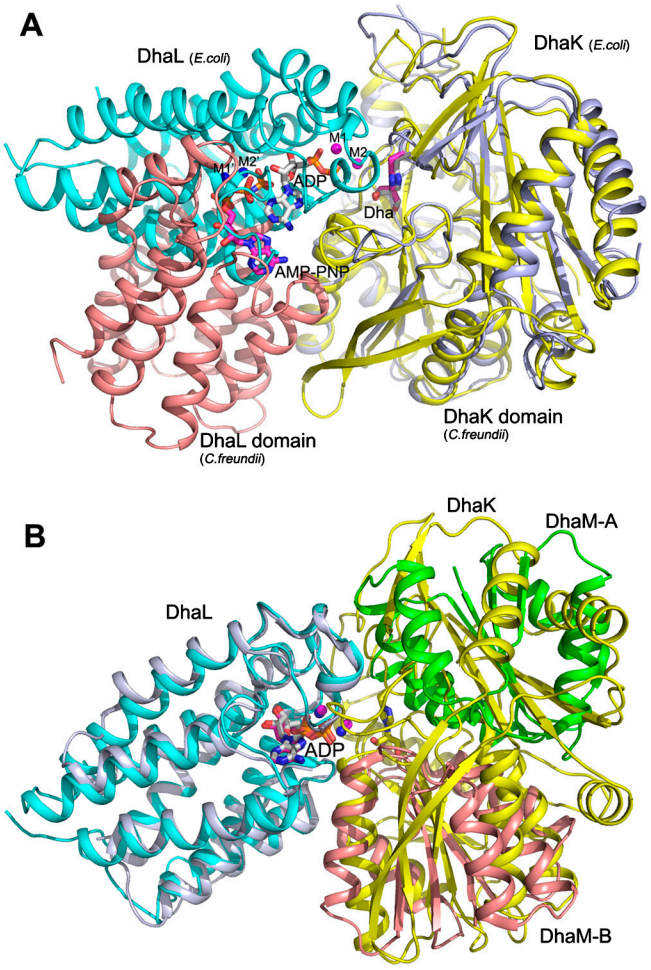

Fig. S1. Superposition of the *E. coli* DhaK–DhaL complex with (*A*) Dha kinase from *C. freundii* and (*B*) the DhaL-DhaM complex from *L. lactis*. Secondary structures are shown in ribbon representation. The AMP-PNP, ADP, and Dha molecules are shown in stick mode and the metal ions as spheres. The *E. coli* DhaK and DhaL subunits are shown in yellow and cyan, respectively. The K- and L-domains from *C. freundii* Dha kinase in (*A*) are shown in light blue and deep salmon, respectively. In *B*, DhaL from *L. Lactis* is colored in light blue and DhaM subunits are colored in green and deep salmon.

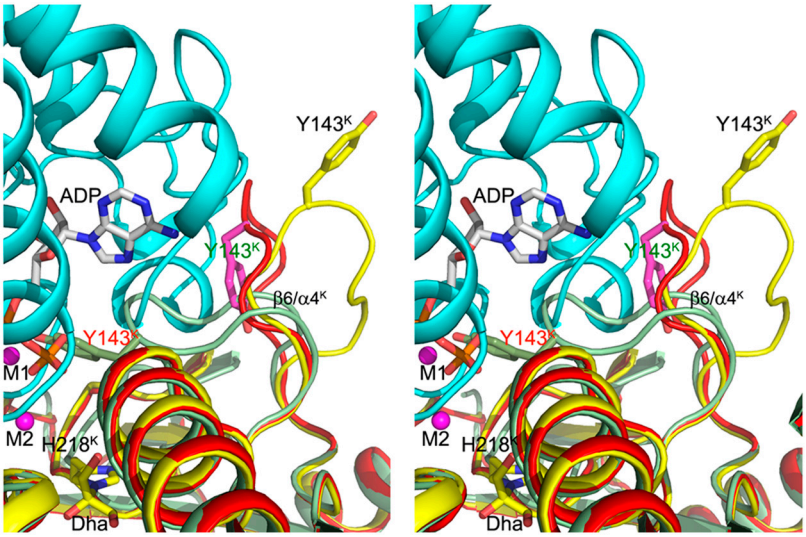

Fig. S2. Conformational flexibility of loop $\beta 6^K/\alpha 4^K$ of DhaK as indicated by three alternate conformations from three crystal structures [DhaK in free form previously determined in space group $P2_12_12$, PDB ID code 1OI2 (10), shown in pale green; DhaK in free form determined in space group $P2_1$ from the current study (PDB ID code 3PNK) is shown in red; DhaK as bound to DhaL (PDB ID code 3PNL) shown in yellow]. Residue $Y143^K$ is shown in stick mode in all three forms. The DhaL from the DhaK–DhaL complex is shown in cyan.

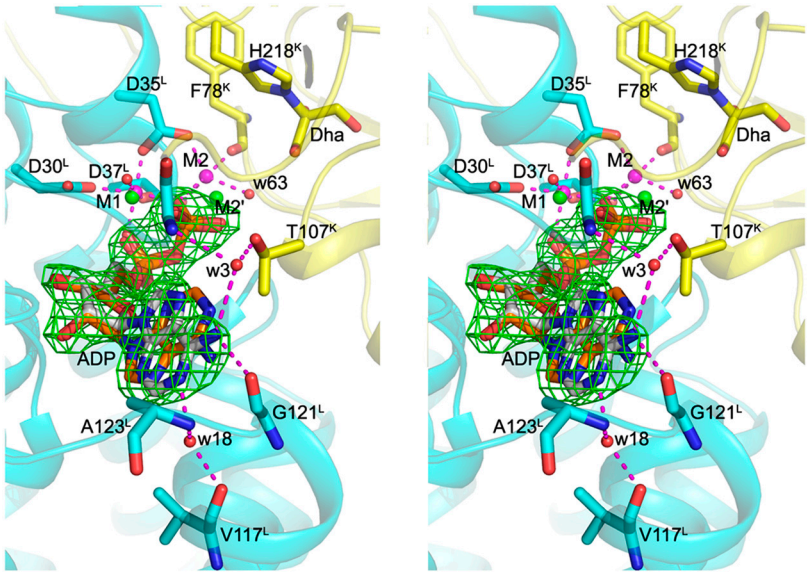

Fig. S3. Conformational change of the ADP molecule (from *syn* to *anti*) and relocation of the second magnesium ion (M2′ to M2) in DhaL upon complex formation. The (Fo – Fc) omit map for the ADP molecule is contoured at 4σ.

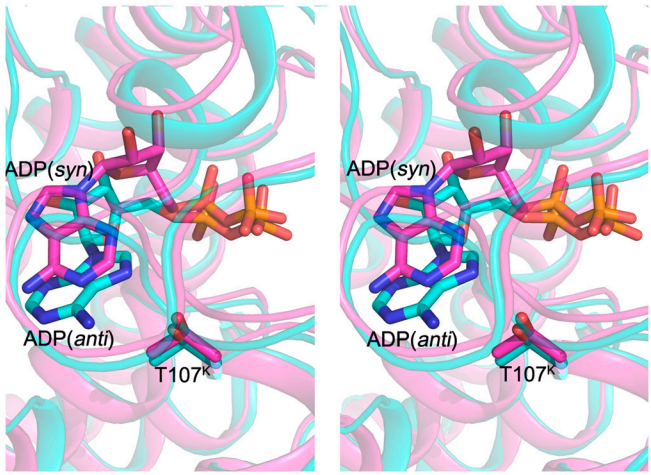

Fig. S4. MD calculation of ADP in both *syn*- (magenta) and *anti*- (cyan) conformations. In all of the resulting models with ADP in the *syn*- conformation, the adenosine moiety of ADP is pushed away due to a potential steric clash with Thr107^{K}.

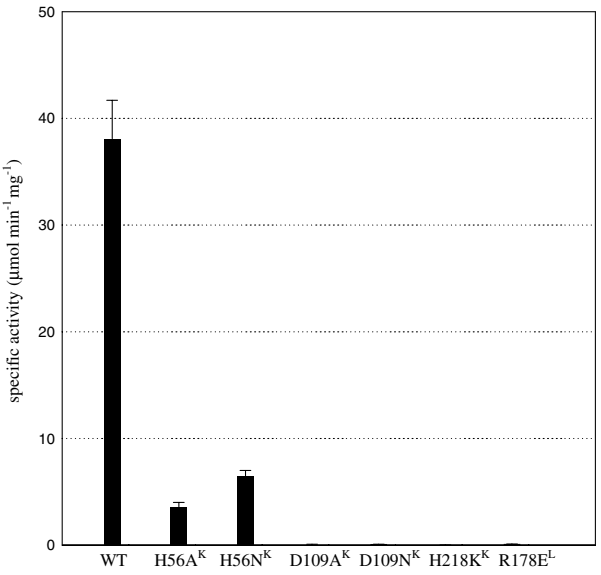

Fig. S5. Specific activity for wild-type Dha kinase and mutants measured at 16 mM Dha. Specific activities are given as μmol Dha-P detectected per minute per mg of DhaL-DhaK protein. The standard deviation was calculated from three independent experiments.

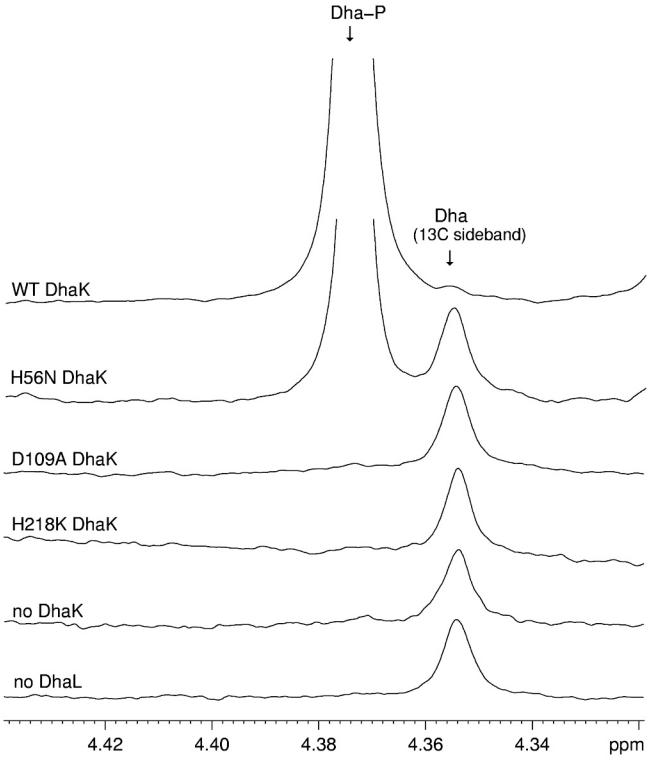

Fig. S6. Representative ^{1}H NMR spectra for Dha-P production by wild-type and mutants of Dha kinase. All spectra were acquired at 23 °C using 2 or 15 min time intervals. Data shown represent 1 hour after reaction was initiated by addition of 3 mM PEP.

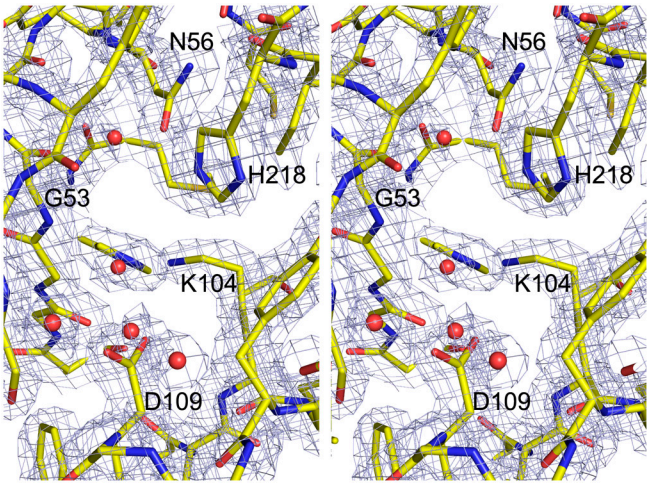

Fig. S7. Active site of the DhaK H56N^{K} mutant. The Dha molecule is absent due to the H56N^{K} mutation. All residues are shown in stick mode and covered by the 2Fo – Fc electron density map contoured at 1.3σ. The residues G53^{K}, N56^{K}, K104^{K}, D109^{K}, and H218^{K} are labeled. Water molecules in close vicinity are shown as red spheres.

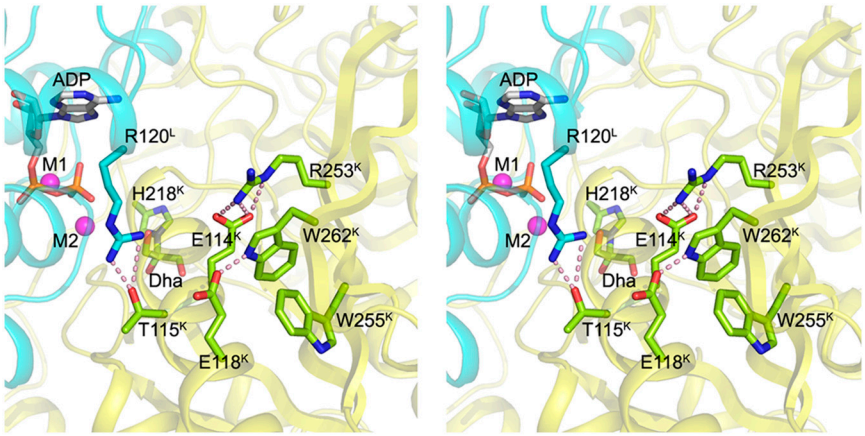

Fig. S8. Anchoring of acidic residues (Glu114^{K} and Glu118^{K}) by residues in the β-hairpin of DhaK, explaining why these residues could not participate in interactions with the DhaL subunit. DhaK is shown in yellow, DhaL in cyan.

Table S1. X-ray data collection and refinement statistics

Data set	DhaK	DhaK–DhaL complex	DhaK (H56A)	DhaK(H56N)	DhaK(H56N)-Dha
Space group	$P2_1$	$P4_12_12$	$P1$	$P1$	$P2_1$
a, *b*, *c* (Å)	49.8, 91.5, 73.2	74.6, 74.6, 268.8	59.8, 82.5, 93.1	59.7, 82.6, 92.9	82.2, 101.1, 99.3
α, β, γ (°)	89.9		77.9, 77.9, 71.0	77.9, 78.1, 71.1	89.95
Wavelength (Å)	0.9793	0.9793	0.9795	0.9795	0.9795
Resolution (Å)*	50–2.21 (2.29–2.21)	50–2.20 (2.28–2.20)	50–2.55 (2.64–2.55)	50–1.97 (2.04–1.97)	50–2.20 (2.28–2.20)
Observed *hkl*	159,649	488,526	153,973	444,133	306,727
Unique *hkl*	30,618	38,172	52,242	111,975	81,917
Redundancy*	5.2 (2.7)	12.8 (7.5)	2.9 (3.0)	4.0 (3.9)	3.7 (3.6)
Completeness (%)*	93.3 (81.1)	96.2 (75.6)	98.7 (98.0)	98.0 (96.9)	99.3 (98.4)
R_{sym} [†]*	0.122 (0.457)	0.091 (0.597)	0.150 (0.508)	0.126 (0.521)	0.086 (0.205)
$I/(\sigma I)$*	10.4 (2.0)	26.1 (2.1)	11 (2.7)	11.5 (2.9)	14.8 (4.8)
Wilson B (Å^2)	30.7	46.9	32.2	15.2	21.7
R_{work} [‡] (# *hkl*)	0.172 (29,018)	0.189 (36,129)	0.172 (49,490)	0.187 (106,318)	0.200 (77,748)
R_{free} (# *hkl*)	0.210 (1,561)	0.225 (1,912)	0.229 (2,657)	0.220 (5,617)	0.221 (4,149)
B-factors (# atoms)					
Protein	30.6 (5,313)	46.4 (4,260)	20.5 (10,273)	17.7 (10,266)	20.4 (10,104)
Solvent	33.5 (165)	44.7 (196)	24.1 (322)	27.6 (1,018)	27.2 (482)
Ligands	24.2 (12)	34.5 (35)	-	-	29.4 (6)
Ramachandran					
Allowed (%)	98.0	99.0	98.7	99.0	98.8
Generous (%)	1.5	1.0	1.0	0.6	0.8
Disallowed (%)	0.5	0	0.3	0.4	0.4
RMSD					
Bonds (Å)	0.011	0.015	0.013	0.009	0.013
Angles (°)	1.35	1.62	1.38	1.20	1.43
PDB ID code	3PNK	3PNL	3PNM	3PNO	3PNQ

*Data for the highest resolution shell are given in parentheses.

[†]$R_{sym} = (\Sigma|I_{obs} - I_{avg}|)/I_{avg}$

[‡]$R_{work} = (\Sigma|F_{obs} - F_{calc}|)/F_{obs}$